# Preparation, characterisation, and application of spent tyre-derived activated carbon chars for total organic carbon removal from wastewater

by M.R. Mulaudzi[1], R.H. Matjie[2], K. Mphahlele[2], J.R. Bunt[2], X. Goso[3], P.O. Osifo[4], K. Premlall[5]

**Affiliation:**
[1]Department of Chemical Engineering Vaal University o\f Technology, South Africa
[2]Centre of Excellence in Carbon-based Fuels, School of Chemical and Mineral Engineering, North-West, University, Potchefstroom Campus, South Africa
[3]Pyrometallurgical Research, Development and Innovation (RDI), Mintek, South Africa
[4]Department of Chemical Engineering Vaal University of Technology, South Africa
[5]Department of Chemical, Metallurgical and Materials, Engineering, Faculty of Engineering and the Built Environment, Tshwane University of Technology, South Africa

**Correspondence to:**
R.H. Matjie

**Email:**
matjie4@gmail.com

**Dates:**
Received: 7 Jul. 2025
Revised: 4 Feb. 2026
Accepted: 9 Feb. 2026
Published: March 2026

**How to cite:**
Mulaudzi, M.R., Matjie, R.H., Mphahlele, K. Bunt, J.R., Goso, X., Osifo, P.O., Premlall, K. 2026. Preparation, characterisation, and application of spent tyre-derived activated carbon chars for total organic carbon removal from wastewater. *Journal of the Southern African Institute of Mining and Metallurgy*, vol. 126, no. 3, pp. 201–216

**DOI ID:**
https://doi.org/10.17159/2411-9717/3768/2026

**ORCiD:**
M.R. Mulaudzi
https://orcid.org/0000-0001-7056-0175
R.H. Matjie
https://orcid.org/0000-0002-2839-3729
K. Mphahlele
https://orcid.org/0000-0003-2677-3928
J.R. Bunt
https://orcid.org/0000-0003-3051-2528
X. Goso
https://orcid.org/0000-0002-6277-9086
P.O. Osifo
https://orcid.org/0000-0001-6539-1266
K. Premlall
https://orcid.org/0000-0003-0917-7585

## Abstract

**This study investigates the transformation of pyrolytic spent tyre-derived char and crumb rubber into high-performance activated carbon chars for industrial wastewater remediation. Utilising an in-house macro-thermogravimetric analysis system under an argon atmosphere, spent tyre-derived activated carbon char were synthesised via physical temperature activation and aqua regia demineralisation. Comprehensive characterisation using x-ray diffraction, Raman spectroscopy, and scanning electron microscopy, revealed a predominantly amorphous structure with nanoscale crystallites (~1 nm) and active surface functional groups. Proximate analysis confirmed that both crumb rubber and leached tyre crumb rubber with aqua regia derivatives achieved favourable compositions (ash ≈ 9.6%; fixed carbon ≈ 84%), comparable to commercial activated carbon (AC). At an optimal activation temperature of 850°C, the char of tyre crumb leached with aqua regia variant exhibited a significant surface area of 300 $m^2/g$. Crucially, the tyre crumb char produced at 850°C variant developed a pore volume of 0.8 $cm^3/g$—effectively doubling that of commercial activated carbon (0.4 $cm^3/g$)—facilitating the sequestration of large organic molecules. In application tests using high-strength starch wastewater, char of tyre crumb leached with aqua regia and tyre crumb char, both produced at 850°C, achieved total organic carbon removal efficiencies of 60% and 50%, respectively, bridging the performance gap between waste-derived and commercial adsorbents. These findings validate waste tyres as a viable, low-cost precursor for industrial-grade adsorbents, offering a sustainable circular economy route for tyre valorisation and reduced industrial disposal costs. Future research will focus on kinetic modelling and the recovery of zinc from spent tyre-derived activated carbon char residues.**

## Keywords

**activation, spent tyre crumb rubber, pyrolytic tyre-derived chars, spent tyre-derived activated carbon chars, activating chemicals, adsorption, wastewater**

## Introduction

The starch manufacturing industry utilises maize and significant volumes of water as primary raw materials to produce starch, gluten, fibre, and germ oil (Tchobanoglous et al., 2003). The resulting starch wastewater (SWW) is classified as "high-strength", due to its elevated concentrations of proteins, lipids, and starches (Ozturk et al., 2005). In South Africa, approximately 640,000 $m^3$ of SWW is discharged annually within the Ekurhuleni Metropolitan Municipality, incurring pre-treatment costs of roughly R16.8 million per year. As highlighted by Sugiati et al. (2023) and Stefanidis et al. (2025), these effluents contain complex organic pollutants, primarily in the form of soluble and suspended solids. If left untreated, these organic loads provide a rich substrate for microbial growth, leading to oxygen depletion in aquatic systems, unpleasant environmental odours, and the spread of water-borne diseases such as cholera and hepatitis (Gorito et al., 2018; Carmona-Cabella et al., 2020).

Simultaneously, the global accumulation of waste tyres—exceeding 1 billion units annually—presents a severe disposal challenge (Liu et al., 2020; López-García et al., 2025). South Africa faces a significant burden, with 2.16 million tonnes of scrap tyres already disposed of and stockpiles increasing by 200,000 tonnes annually (Nkosi et al., 2025). During the pyrolysis of these tyres, approximately 30% – 35% by weight is converted into pyrolytic tyre-derived char (PTDC), a by-product composed of carbon, metals, and inert materials (Muzenda, 2014). Given the abundance and high carbon content of PTDC—derived from the carbon black used as a reinforcing filler—there is a critical need for its valorisation. Reprocessing PTDC into spent tyre-derived activated carbon char (STACC) offers a sustainable circular economy solution for treating industrial wastewater.

While commercial granular steam-activated carbons are widely used for pollutant removal, their reliance on non-renewable precursors like coal or wood has prompted a shift toward waste-derived alternatives (Ali et al., 2012; Wang et al., 2009). Yu et al. (2019) demonstrated that pyrolysing carbonaceous materials at temperatures between 800°C and 900°C yields activated chars with specific pore size distributions suitable for wastewater remediation. Their work established that chemical activation often achieves higher surface areas compared to physical methods. Furthering this, Ayaz et al. (2025) introduced "greener" organic activating agents, such as sodium oxalate, to produce porous carbons with surface areas reaching 1630 $m^2/g$.

Specifically regarding tyre-derived materials, Muttil et al. (2023) utilised a variety of chemical agents, including potassium hydroxide (KOH), zinc chloride ($ZnCl_2$), and phosphoric acid ($H_3PO_4$), and physical steam activation to produce STACCs with surface areas up to 928 $m^2/g$. These materials proved highly effective in removing organic dyes such as methylene blue and malachite green from aqueous solutions. Similarly, foundational studies by Cunliffe and Williams (1998) and recent investigations by Abbas-Abadi et al. (2022) and Zhang et al. (2024) have confirmed that the physico-chemical properties of tyre-derived chars can be significantly improved through targeted activation protocols.

Despite these advancements, a mechanistic understanding of how activation influences the performance of tyre-derived chars, specifically for high-strength starch wastewater, remains limited. Furthermore, there is a lack of literature regarding the use of aqua regia (AR) as a demineralisation pre-treatment for South African pyrolytic chars. This study addresses this gap by investigating the preparation of STACCs using a dual approach: physical activation temperature and a preparatory chemical leaching step using an aqua regia solution (3:1 HCl:$HNO_3$). The primary objective is to evaluate the efficiency of these STACCs in removing total organic carbon (TOC) from starch wastewater, providing a sustainable route for tyre waste valorisation and reduced industrial disposal costs.

## Materials and methods

### *Chemicals and gases*

Hydrochloric acid (HCl) (35%) and nitric acid ($HNO_3$) (65%) were supplied by Protea Laboratory Solutions (Pty) Ltd. In this study, an AR solution was prepared by carefully mixing 1 $dm^3$ of 65% concentrated $HNO_3$ with 3 $dm^3$ of 35% concentrated HCl in a 5 $dm^3$ beaker under a fume hood. The resulting mixture was stirred thoroughly using a magnetic stirrer to ensure homogeneity. AR was employed solely to dissolve mineral matter present in the PTDC or spent crumb rubber (TC), thereby adjusting the ash percentage yield of the feedstock prior to activation testing. It is important to note that the use of AR is not part of the proposed STACC production technology for wastewater treatment applications but was applied only as a preparatory step in this experimental study.

It is known that these chemical activating agents stated in the aforementioned can form acidic reactive sites on solid samples during activation of the carbon-containing materials to produce activated carbons (AC) or adsorbents (Danish et al., 2013). In addition, these activating agents contribute positively to the augmentation of the Brunauer–Emmett–Teller specific surface area (BET SA) with surface adsorption sites increasing their adsorption capability of organic and inorganic pollutants from wastewater (Bai et al., 2024).

Argon gas (99.99%) was sourced from African Oxygen (Afrox) Ltd, South Africa and used to create an inert atmosphere during the activation experiments of TC, PTDC, either TC or PDTC leached with AR at different elevated temperatures to produce STACCs. The measured physical properties of these produced ACCs included BET SA and pressure volume (PV) for the adsorption of organic compound pollutants from wastewater. These will be augmented during the activation tests in a macro- thermogravimetric analysis (macro-TGA).

### Sample collection and preparation

Spent tyre crumb rubber (TC) is a granular material derived from recycled or spent car tyres. A magnet was used to remove significant amounts of metal pollutants from the recycled car tyres prior to the pyrolysis tests of TC to produce pyrolytic spent tyre-derived char (PTDC). The representative PTDC sample (about 20 kg) with a particle size ranging from 0.9 mm to 5 mm was taken from the Energy Partners pyrolysis plant in Alrode, South Africa, and the representative TC (20 kg) sample was supplied by Dawhi rubber-recycling company located in Germiston, South Africa. The sampling campaign for the PTDC and TC representatives was conducted by adopting the International Organisation for Standardisation (ISO) guidelines in ISO18283 and ISO 13909-4 standards. In addition, 5 kg of commercial granular Aqua-Sorb 1200 commercial activated carbon (AC), as the experiment control, with a particles size ranging from 2 mm to 5 mm was used in this study and was sourced from UDEC Trading (Pty) Ltd., Kempton Park, South Africa. A total of 20 $dm^3$ (representative) of starch wastewater (SWW), with a concentration of 25 357 ppm and pH of 4.6, was sampled at a corn-starch processing plant in Germiston, South Africa, by following the procedures stipulated in ISO 5667-21 (2010). The bulk samples were stored in an argon atmosphere, and chilled to minimise UV interference and decomposition during storage.

Either PTDC or TC was leached with aqua regia (AR) at room temperature using a solid to liquid ratio of 1:3 for 4 days to generate the acid leached residues for the activation tests to produce char for purification of SWW. All mixtures of AR and either PTDC or TC were agitated at 500 revolutions/minute (rpm). These residues were separated from the leach liquor using a normal filtration. They were subsequently washed with sufficient deionised water to remove some dissolved inorganic species. The acidic leached residues were dried at 50°C for 24 hours and then stored in an argon atmosphere prior to the activation tests. The samples activated in the macro-thermogravimetric analysis (macro-TGA) for improving physical properties (surface area and pore volume) were labelled as follows: A is pyrolytic spent tyre-derived char (PTDC); H is PTDC residue leached with Aqua regia; spent tyre crumb rubber (TC), and TC leached with aqua regia (TCA).

### Experimental design

A systematic experimental design was employed to evaluate the impact of feedstock pre-treatment and activation temperature on the performance of the resulting spent tyre-derived activated carbon chars ( STACCs). The study followed a 2 x 2 factorial approach focusing on two primary variables: (1) Feedstock type (raw tyre crumb vs. de-mineralised tyre crumb) and (2) Activation methodology (physical vs. chemical). All activation experiments were performed in an argon atmosphere to maintain inert conditions. The specific experimental runs and their corresponding conditions are summarised in Table 1.

*Table 1*
**Consolidated experimental design for STACC production**

| Run ID | Feedstock type | Pre-treatment (leaching) | Temperature (°C) | Target Metric |
|---|---|---|---|---|
| TC1 | Tyre crumb (raw) | None | 650 | Initial porosity |
| TC2 | Tyre crumb (raw) | None | 850 | Max pore volume |
| TCA1 | Tyre crumb (leached) | AR | 650 | Ash reduction |
| TCA2 | Tyre crumb (leached) | AR | 850 | Max surface area |
| AC | Commercial carbon | N/A | N/A | Control |

## Thermal activation of PTDC, TC, and acid leached TC/PTDC

The activation experiments were conducted using a custom-built macro-thermogravimetric analysis (macro-TGA) system at the Council for Mineral Technology (MINTEK), South Africa. The macro-TGA apparatus comprises a vertical tube furnace fitted with a high-purity alumina reactor tube (internal diameter: 6 cm; height: 0.9 m) (Baloyi, et al., 2025). Heating was provided by molybdenum disilicide ($MoSi_2$) elements, ensuring stable and uniform temperature control. The test crucible, also made of alumina, was cylindrical with an internal diameter of 3 cm and a height of 4.5 cm. A schematic representation of the macro-TGA system is presented in Figure 1.

Activation experiments were performed at target temperatures of 450°C, 650°C, and 850°C, which were selected based on literature reports indicating that surface area (SA) and pore volume (PV) increase with temperature up to approximately 850°C, beyond which both parameters decrease significantly (Howaniec, 2016).

Approximately 10 g – 30 g of each sample (A, TC, TCA, or H) was loaded into the crucible located in the sample compartment of the furnace. The system can accommodate sample masses ranging from 10 g to 50 g per experiment. The crucible was mounted on a pedestal connected to a precision thermo-balance for continuous measurement of mass loss.

Temperature and sample weight were recorded every 10 seconds via the data acquisition system. The furnace temperature was ramped to the selected set point (450°C, 650°C, or 850°C) at a rate of 10°C $min^{-1}$, following the methodology adopted in previous studies that demonstrated the suitability of these temperatures for producing activated adsorbents (Han, et al., 2023). Upon reaching the final temperature, the samples were held isothermally for 4 hours before being cooled under an argon atmosphere to prevent oxidation.

The selection of 850°C as the upper activation limit was based on the findings of Muttil et al. (2023), who observed that tyre-derived carbon structures undergo optimal pore enlargement at this temperature, whereas temperatures exceeding 900°C may cause structural sintering. The activation time of 1 hour was maintained across all runs to ensure complete volatilisation of residual organics without compromising the mechanical integrity of the char particles.

The resultant activated char samples were stored under argon and designated as follows: PTC1 (A activated at 650°C), PTC2 (A activated at 850°C), TC1 (TC activated at 450°C), TC2 (TC activated at 850°C), ARC1 (H activated at 650°C), ARC2 (H activated at 850°C), and TCA2 (TCA activated at 850°C). Representative tyre crumb (TC) and pyrolytic tyre-derived char (PTDC) samples, along with their activated counterparts, were prepared according to the International Organization for Standardization (ISO) protocols (ISO 18283; ISO 13909-4). These materials were subsequently subjected to various physicochemical and structural analyses.

In this investigation, both the novel activation and adsorption experiments and analytical results were conducted in triplicate, and the error of the replicate tests was determined, based on the standard deviation for tests or analytical results for the samples, and a 95% confidence interval was used to recognise significant changes. Furthermore, the average results for the samples from the different analytical techniques followed in this study are reported. Error bars are shown on all figures. A confidence interval for each product fraction was calculated using Equation 1.

$$CI = \bar{x} \pm (t_{score} \times \frac{\sigma}{\sqrt{n}}) \quad [1]$$

Where:
$\bar{x}$ refers to the sample mean, $\sigma$ is the standard deviation and $n$ is the sample size (in this case 3). The $t_{score}$ = 4.303 for 2 degrees of freedom and a 95% confidence level.

## Procedure for adsorption studies

Adsorption experiments were performed in batch mode using a fixed-bed adsorption column with an internal diameter of 40 mm, empty bed of 2.45 $cm^3$, and height of 400 mm packed with chars, with commercial activated carbon (AC) serving as the control material at 23°C (Figure 2). The experimental setup comprised an adsorption tube, a peristaltic pump, and a sample holder (Kuśmierek et al., 2021; Igwegbe et al., 2021; Mohammed et al., 2023; Jiang et al., 2024). Starch wastewater (SWW) was pumped at 3.3 ml/min using a Minibus 3 (Gilson) peristaltic pump through a 3 mm internal diameter delivery tube into the adsorption column, which had a total height of 450 mm and an internal bed volume of 2.45 $cm^3$.

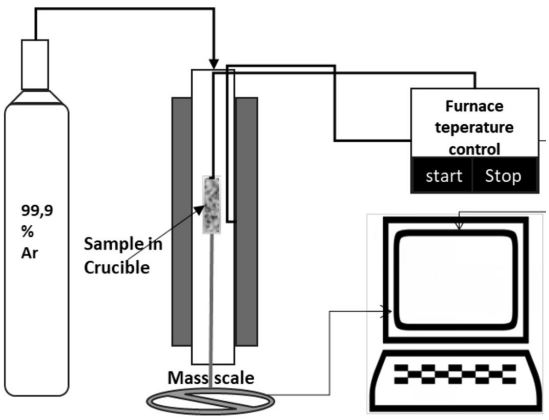


**Figure 1—Schematic diagram of macro-TGA set-up (Baloyi et al., 2025)**

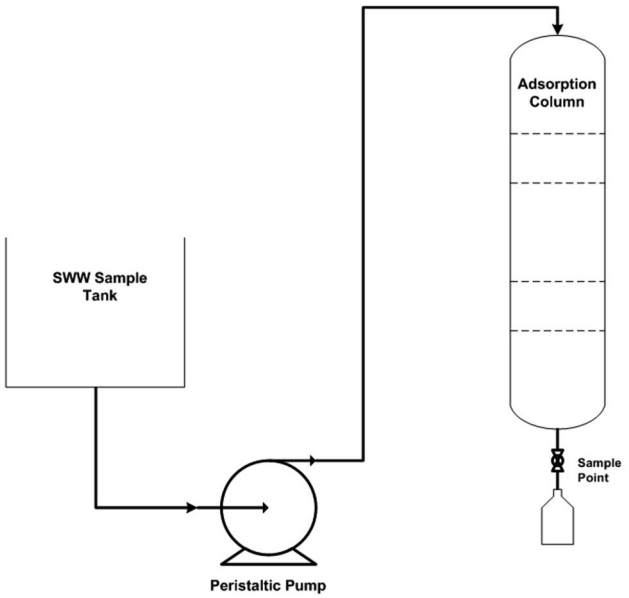


**Figure 2—Adsorption of organic impurities from wastewater using different produced adsorbents**

The column was packed with either activated carbon char (ACC) or commercial activated carbon (AC) to compare adsorption performance. A plastic distribution plate with 200 µm perforations was positioned at the top of the column to ensure uniform flow distribution of the influent. At the base, a 2 mm spacing was occupied by filter paper (volume = 2.45 $cm^3$) with a pore size of 50 µm to prevent solid loss. Above this, approximately ±15 g of activated char was loaded, while the top 5% of the column volume was left void to accommodate flow dynamics.

To assess the influence of empty bed contact time (EBCT) on total organic carbon (TOC) removal efficiency using TCA2, the EBCT varied from standard operational conditions to simulated challenge conditions. Under normal operating conditions, the EBCT was maintained at 60 minutes, representing the long-term design value for this treatment system. During challenging conditions—such as bed overflow, clogging, and channel formation—the EBCT was reduced to approximately 30 minutes (Figure 2), while a parallel reference column was maintained at 60 minutes for comparison.

SWW was introduced into the column at a constant flow rate of 3.3 mL/min, corresponding to a hydraulic residence time of 30 minutes. Effluent samples were collected after each adsorption run for subsequent characterisation. Residual SWW was drained, and the remaining liquor was weighed to calculate the adsorption capacity. To characterise the total organic carbon (TOC), the content of samples of SWW and effluent were analysed using a Teledyne-Tekmar TOC Torch analyser.

## Uncertainty for total organic carbon removal percentage and equilibrium

The main sources of uncertainty in the determination of total organic carbon (TOC) removal efficiency during adsorption experiments were associated with the measurement of adsorbent mass, solution volume, and the determination of final TOC concentration (Zilli, 2013; Yang et al., 2020). The principal contributors were the weighing accuracy of the analytical balance (15 g ± 1.5 g) and the potential reading error introduced by the concave meniscus during volumetric measurements of the final solution. Although these uncertainties were relatively small, their combined effect could influence the calculated TOC removal efficiency, particularly in cases involving low adsorbent capacities such as SWW–TOC.

The adsorption performance of the synthesised STACCs was evaluated through batch equilibrium tests. The removal efficiency (RE) and the equilibrium adsorption capacity ($q_e$, mg/g) were calculated using the following mass-balance equations (Equations 2 and 3):

$$\mathrm{RE} = \frac{C_o - Ce}{C_o} \times 100 \quad [2]$$

$$\mathrm{qe} = \frac{C_o - C_e}{\mathrm{m}} \times V \quad [3]$$

Where $C_0$ and Ce are the initial and equilibrium TOC concentrations, (mg/L) is the volume of the solution (L), and m is the mass of the adsorbent (g).

## Characterisation study of samples

The proximate analyser (Ultra Furn SVF 11/15/14N for the volatile determination, Ultra Furn SAF 11/1/P4 for the ashing, Ultra Furn UMFSO/1 minimum free space oven for the moisture determination, Ultra Furn UMFSD/1 desiccator for the moisture determination, LECO SC632 for the sulphur determination, and LECO SC832DR for the sulphur determination) and ultimate analyser (Leco TruSpec CHN) characterised the pulverised AC and TC/A/H/TCA and their STACCs using ISO standard methods for coal analyses (Rautenbach et al., 2019) at Bureau Veritas Laboratory, South Africa. Proximate and ultimate results for these samples presented and discussed in this paper are semi-quantitative and must be considered with some care.

A North-West University (NWU) XRF spectrometer (PANalytical Axios Max) determined proportions of inorganic elements in the ashes derived from the produced samples (<75 µm), i.e., AC, PTDC, H, TC, chars from PTDC produced at 450°C, 650°C, and 850°C, ARC1, ARC2, TC1, TC2, and TCA2. The XRF analysis was conducted at the NWU (ASTM D4326-13) (Norrish, Hutton, 1969). Either AMIS or WROXI standards could be used to calibrate an XRF spectrometer at NWU, depending on the specific application. AMIS provides certified reference materials (CRM) for a wide range of natural mineral samples, whereas WROXI is a set of synthetic standards for general oxide analysis.

The quantitative and qualitative XRD analysis methods of AC and A, H, and their chars (<75 µm), were carried out at the XRD Analytical & Consulting Laboratory in Pretoria, South Africa using the Malvern Panalytical Aeris – research – edition XRD equipment equipped with a Co x-ray tube as well as an X'Celerator detector, with Rietveld-based X'Pert HighScore Plus Software and an International Centre for Diffraction Data (ICDD) program (Rietveld, 1969; Speakman, 2012). Silicon powder certified reference materials (CRM), such as those in the NIST SRM 640 series, are widely used to calibrate x-ray diffraction (XRD) equipment and ensure measurement precision. Malvern Panalytical, a supplier of XRD instruments, offers these NIST-certified standards through its online store. Also, the selected TC1, TC2 and TCA2 samples were submitted for the qualitative XRD analysis. Moreover, the AC and STACCs (TC1, A, AC, TCA2, and TC2) were submitted for the determination of their crystallite size, crystalline height, and graphitic carbon content. The Scherrer equation was used to

estimate the crystallite size of carbon using the corresponding full width at half-maximum (FWHM) parameters of the graphite peak on the XRD diffractograms (Scherrer, 1912; Patterson, 1939).

The Raman analysis of the produced chars ($ARC_1$, $ARC_2$) and AC was conducted at the University of Johannesburg, South Africa, using a WITec Alpha 300R Confocal Raman spectrometer, equipped with a 532 nm laser and a 50× objective. The instrument calibration involves spectral calibration using a known standard like silicon or a mercury-argon lamp to accurately map wavelengths to detector pixels (x-axis calibration) and a known silicon peak to set the zero and 520.7 $cm^{-1}$ peak positions (y-axis/Raman shift calibration). A detailed description of the equipment and the method used can be found elsewhere (Kapesi, 2018). The Raman spectra obtained were processed using Origin Lab 2019 software. A detailed description of the equipment and the method used can be found in Kapesi (2018).

The surface areas of the selected produced chars were determined by means of nitrogen adsorption experiments using a TriStar II instrument (Micromeritics, USA) ASAP 2010 Analyser at the North-West University to analyse the structural features of adsorbent materials. Initially the samples were degassed at 110°C for a period of 48 hours. After degassing, the char samples were analysed by means of gas adsorption using nitrogen as a sorbent. All of the gas adsorption experiments were conducted at a temperature of -196°C using a saturation pressure ($P_0$) of < 660 mm Hg.

The SEM analysis was conducted at the Council for Scientific and Industrial Research (CSIR) using a piece of double-sided conductive carbon tape on the stub containing the char sample coated with iridium (Ire) for conduction purposes. Microscopy and other image-based measurement systems' instruments are calibrated twice a year by suppliers using samples with known distances to ensure measurement accuracy. This process compares the instruments' measurements to a reliable standard and adjusts for any inconsistencies or drift. The sample was viewed using a Jeol-JSm-6010 analytical SEM connected to InTouch Scope software with magnification setting for final image.

The performance of each char produced in this study was evaluated by analysing the SWW permeate collected during the adsorption experiment. The samples were first filtered using a 0.45 µm filter paper. The TOC was analysed using a TOC analyser (Teledyne-Tekmar TOC Torch analyser) supplied by Ingrain South Africa, which was used to determine the TOC concentration in the SWW permeate. The instrument uses ion chromatography (882 CompactIC Plus fitted with an 863 Compact auto sampler) (Aoyi et al., 2017).

## Results and discussion

The char compositions of commercial activated carbon and spent tyre crumb rubber in pyrolytic spent tyre-derived char, pyrolytic spent tyre-derived char leached with aqua regia, and spent tyre crumb rubber leached with aqua regia samples

The proximate and ultimate analysis results for samples labelled commercial activated carbon (AC), spent tyre crumb rubber (TC), pyrolytic spent tyre-derived char (A), pyrolytic spent tyre-derived char leached with aqua regia (H), and spent tyre crumb rubber leached with Aqua regia (TCA), along with their corresponding spent tyre-derived activated carbon chars (STACCs), are presented in Table 2. Among all samples tested, commercial activated carbon (AC) exhibited the highest fixed carbon content and the lowest ash yield, outperforming both the raw feedstock materials and their respective STACCs used in the adsorption experiments. The raw char samples TC and TCA displayed the highest volatile matter (VM) content among all samples analysed. In contrast, the TCA2 sample (produced by leaching spent tyre crumb rubber with aqua regia) exhibited a higher inherent moisture content and lower VM content compared to commercial activated carbon (AC). Notably, STACCs derived from TC and H (specifically TCA, TC2, and ARC1) showed significantly elevated moisture contents, consistent with the trend observed across other STACC samples. This increase in moisture content is attributed to the surface oxidation of rubber in TC and PTDC by nitric acid present in aqua regia, leading to the formation of hydrophilic functional groups such as carbonyl (-COOH) moieties on the char surfaces (Chen, Wu, 2004).

As expected, the pyrolytic tyre-derived chars from the H sample activated at 650°C (ARC1) exhibited relatively higher volatile matter content compared to those activated at 850°C (ARC2 and TCA2). The reduction in volatile matter observed in TCA and H samples at elevated activation temperatures was accompanied by a notable increase in fixed carbon content and ash yield (% AY). These findings are consistent with previously reported data on South African waste tyre-based activated carbon chars (ACC) by Maapola (2019). Additionally, Li et al. (2005) reported high ash yields (ranging from 10.6 wt.% to 14.7 wt.%) in activated carbons derived from Chinese and Canadian waste tyres, produced at varying temperatures (450°C to 650°C) using different reactor systems. The relatively higher ash yield percentage observed in the South African STACCs is attributed to the presence of mineral matter, including remnants of metal wires, sulphonic acid residues, processing oils, and inorganic additives such as Zn, Fe, Ni, Cu, V, S, and $SiO_2$, commonly found in spent tyre char (TC) samples (Maapola, 2019; Rodriguez et al., 2017).

The ultimate analysis results, presented in Table 1, show that AC contains a lower carbon content compared to all other samples, except for TCA. Additionally, AC exhibited the lowest total sulphur (TS) content among all samples analysed. The relatively high carbon and sulphur contents observed in the spent tyre material, PTDC, and their corresponding STACCs are primarily attributed to the presence of carbon black, sulphonic acids, operating oils, and sulphur compounds inherent in the original tyre char (TC) samples (Rodriguez et al., 2017). Furthermore, during activation, organic vapours released from the TC samples may condense on the surface of the activated chars, thereby contributing to an increase in surface carbon content (Martinez et al., 2013).

It is known that metal species such as Zn/ZnO and Fe/FeO/Ni/Cu/V present in the char matrix can react with sulphur (S) to form stable metal sulphides, including ZnS, (Zn,Fe)S, and Fe/Ni/Cu/V sulphides, thereby retaining a portion of the sulphur species within the STACCs (Yaru et al., 2021). In contrast, gaseous sulphur-containing compounds, such as hydrogen sulphide ($H_2S$), may volatilise from the TC samples during high-temperature activation, contributing to a reduced total sulphur (TS) content in the resulting STACCs compared to the original TC material. The TS content in tyre-derived samples generally decreases with increasing activation temperature. A comparatively higher nitrogen (N) content observed in the TCA (TC leached with AR) and TCA2 samples is likely due to residual nitric acid or nitrate species adsorbed onto the sample surfaces, as well as nitrogen-containing components originating from operating oils in the original TC (Seng-Eiad, Jitkarnka, 2016). These authors reported the presence of nitrogen-containing functional groups such as C–N bonds from aromatic amines, which possibly contribute to the elevated nitrogen content in the STACCs. Nitric acid may also react with aromatic structures in TC, such as benzene rings, leading to the formation of nitrobenzene groups in

*Table 2*

**Average proximate and ultimate results of AC and TC/A/H/TCA and spent tyre-derived ACCs produced at elevated temperatures (wt. %)**

| Samples | Proximate results (wt. % adb) | | | | Ultimate results (wt. % adb) | | | | |
|---|---|---|---|---|---|---|---|---|---|
| | IM | AY | VM | FC[i] | C | H | N | O[i] | TS |
| **AC** | 3.1 | 5.0 | 5.0 | 86.9 | 74.9 | 3.0 | 0.4 | 21.3 | 0.3 |
| **TC** | 0.5 | 6.1 | 64.5 | 28.9 | 82.1 | 7.2 | 0.5 | 1.8 | 8.4 |
| **TCA** | 2.5 | 8.0 | 52.8 | 36.7 | 69.7 | 5.7 | 2.4 | 20.9 | 1.3 |
| **TC1** | 1.1 | 17.1 | 3.4 | 78.4 | 80.1 | 0.5 | 0.3 | 16.5 | 2.9 |
| **TC2** | 2.8 | 10.1 | 3.5 | 83.6 | 84.2 | 0.5 | 2.1 | 12.1 | 1.1 |
| **TCA2** | 3.4 | 9.6 | 2.9 | 84.1 | 84.5 | 0.7 | 2.2 | 11.6 | 1.1 |
| **A** | 1.0 | 13.2 | 4.0 | 81.8 | 93.1 | 0.8 | 0.5 | 2.3 | 3.3 |
| **PTC1** | 1.9 | 13.0 | 2.2 | 82.8 | 93.0 | 0.5 | 0.5 | 2.8 | 3.3 |
| **PTC2** | 1.1 | 12.2 | 1.6 | 85.1 | 92.8 | 0.6 | 0.5 | 3.0 | 3.2 |
| **H** | 6.8 | 10.3 | 14.3 | 68.6 | 91.4 | 3.2 | 0.9 | 3.4 | 0.9 |
| **ARC1** | 2.7 | 10.9 | 4.0 | 82.3 | 90.0 | 0.5 | 0.7 | 7.9 | 0.9 |
| **ARC2** | 1.3 | 11.5 | 1.9 | 85.3 | 90.3 | 0.5 | 0.6 | 7.9 | 0.8 |

"Daf—dry ash-free basis, adb—air-dried basis, IM—inherent moisture, AY—ash yield, VM—volatile matter, FC—fixed carbon, TS—total sulphur",
"i" — determined by calculation.
AC—commercial activated carbon; TC—tyre crumb rubber; TCA—leached tyre crumb rubber with AR; TC1—tyre crumb char produced at 450 °C; TC2—tyre crumb char produced at 850 °C; TCA2—char of tyre crumb leached with AR produced at 850 °C; A—PTDC; PTC1—char of PTDC produced at 650 °C; PTC2—char of PTDC produced at 850 °C; H—PTDC leached with AR; ARC1—char of leached PTDC with AR produced at 650 °C; ARC2—char of PTDC leached with AR produced at 850 °C.

the activated chars. Both TC and TCA exhibited higher H content relative to the other samples. This is attributed to the presence of unsaturated hydrocarbons (alkenes), sulphonic acids, aromatic compounds, and polycyclic aromatic hydrocarbons (PAHs) from residual oils in the rubber matrix (Maapola, 2019). Furthermore, AC and TCA displayed significant oxygen (O) content when compared to the other samples. The elevated O content in TCA is associated with nitric acid or nitrate residues from AR treatment, as well as the formation of oxygen-containing polar functional groups on the rubber crumb surface during activation (Xiaowe et al., 2017). According to He et al. (2016) nitric acid treatment increases the O content in rubber-derived chars and induces surface polarity by introducing oxygenated functionalities.

The proximate and ultimate analysis results offer valuable insight into the selection of suitable carbon-containing feedstocks for the production of activated carbons, particularly based on their ash yield (%) and carbon content. These characteristics are critical, as they influence both the yield and performance of the resulting activated carbons in various applications, including the adsorption of impurities from wastewater, gold recovery, metallurgical processes (iron, titanium, and steel production), the food manufacturing industry, and gasification technologies. Ash yield and fixed carbon (FC) content are especially pivotal in determining the adsorption behaviour and overall quality of the produced activated carbons (Rambau et al., 2018). According to Zhang et al. (2019) feedstocks with percentage ash yield exceeding 10% typically produce activated carbons with larger surface areas during the activation process. Furthermore, carbonaceous materials with FC contents greater than 32% tend to yield higher quantities of activated carbon upon activation (Daniel et al., 2023).

### X-ray fluorescence analysis of control samples

Table 3 presents the chemical composition of the ashes derived from control sample AC and samples A, TC, H, and TCA, and their STACCs produced at 450°C, 650°C and 850°C. The proportions of inorganic elements present in the ash samples determined using x-ray fluorescence (XRF) analysis are reported as inorganic elemental oxides. It can be seen that ashes of Sample A are constituted primarily of $SiO_2$ and ZnO. Also, lesser proportions of $Fe_2O_3$, $K_2O$, $SO_3$, $Al_2O_3$, and CaO were detected along with the traces of MnO, $P_2O_5$, $TiO_2$, and NiO in the ash samples of STACCs and AC. Moreover, ARC1 and ARC2 contained lower proportions ZnO, $Al_2O_3$, and $Cr_2O_3$ along with traces of other inorganic elements. The reduction of the concentrations of these inorganic elements in the ARC1 and ARC2 was due to the dissolution of these inorganic elements from A with AR. On the other hand, the ash composition of AC constituted major proportions of $SiO_2$ and $Al_2O_3$ along with minor proportions of $Fe_2O_3$, $K_2O$, CaO, MgO, $P_2O_5$, $TiO_2$, and traces of NiO, $SO_3$ and $Cr_2O_3$, which could be associated with amorphous aluminosilicate phases and quartz present in this sample. The ash of sample ARC1 contained a lower proportion of $SiO_2$ and high proportions of $Fe_2O_3$ and $Cr_2O_3$ due to the corrosion of the stirrer equipment containing Fe and Cr metals together with AR during leaching. Higher proportions of major inorganic elements including ZnO and $SiO_2$ in the ashes of activated PTDC samples are attributed to the decomposition of organic matter for chars in the PTDC samples based on the loss in ignition determination at elevated temperatures for the XRF analysis. The presence of ZnO, $SiO_2$, S, Mg as well as $Fe_2O_3$ in the ashes of spent tyre and their chars is ascribed to inorganic additives (zinc metal or ZnO, $SiO_2$, S; Fe metal, Mg and Si from steel wire) originally contained in TC (Rodriguez et al., 2017; Agblevor et al., 2024). In

*Table 3*

**Average chemical composition of ashes of AC and TC, PTDC, A, and H, and their corresponding STACCs (w/w %)**

| Inorganic elements | AC | A | PTC1 | PTC2 | H | ARC1 | ARC2 | TC1 | TC2 | TCA2 |
|---|---|---|---|---|---|---|---|---|---|---|
| $SiO_2$ | 62.2 | 44.8 | 34.1 | 55.3 | 52.1 | 32.5 | 62.1 | 53.6 | 67.8 | 58.5 |
| ZnO | 0.6 | 39.0 | 45.3 | 30.0 | 1.4 | 0.7 | 0.4 | 30.9 | 14.7 | 22.1 |
| $Fe_2O_3$ | 5.4 | 3.9 | 9.1 | 2.3 | 29.7 | 47.1 | 18.8 | 1.2 | 3.1 | 1.8 |
| $K_2O$ | 1.9 | 1.4 | 2.2 | 1.7 | 0.6 | 1.1 | 4.7 | 1.6 | 1.2 | 2.4 |
| $Al_2O_3$ | 20.7 | 3.6 | 3.4 | 4.8 | 3.6 | 2.0 | 4.0 | 5.5 | 7.5 | 7.1 |
| CaO | 2.6 | 2.1 | 2.5 | 2.4 | 0.4 | 0.3 | 0.4 | 4.6 | 3.3 | 5.6 |
| $Cr_2O_3$ | 0.6 | 0.3 | 0.2 | 0.2 | 7.3 | 11.3 | 5.8 | 0.0 | 0.3 | 0.1 |
| MgO | 1.3 | 1.3 | 1.1 | 1.3 | 0.8 | 0.5 | 0.5 | 1.1 | 1.0 | 1.0 |
| $P_2O_5$ | 1.4 | 0.7 | 0.5 | 0.3 | 0.1 | 0.1 | 0.0 | 1.2 | 1.0 | 1.1 |
| $TiO_2$ | 1.8 | 0.3 | 0.3 | 0.4 | 0.3 | 0.2 | 0.4 | 0.3 | 0.5 | 0.3 |
| NiO | 0.3 | 0.1 | 0.1 | 0.1 | 3.0 | 0.0 | 2.5 | 0.0 | 0.1 | 0.0 |
| $SO_3$ | 0.7 | 1.5 | 0.0 | 0.0 | 0.1 | 0.0 | 0.0 | 0.0 | 0.0 | 0.0 |
| Total | 100.0 | 100.0 | 100.0 | 100.0 | 100.0 | 100.0 | 100.0 | 100.0 | 100.0 | 100.0 |

addition, the chemical composition of ashes of these samples are in good agreement with the x-ray diffraction (XRD) results for the A, TC, and their chars. The XRF results are consistent with previous chemical composition data of waste tyre-derived ashes (Maroufi et al., 2017). Furthermore, the recovery of high-value inorganic elements including Zn should be investigated utilising hydrometallurgical methods (acid and base leaching steps).

## X-ray diffraction analysis

The XRD results for AC and A, and H and TC samples along with their corresponding STACCs are presented in Tables 4 and 5, and Figure 3 and Figure 4. The AC sample contained the lowest mineral matter (MM) content in relation to all samples analysed. The XRD analysis detected quartz and higher proportions of amorphous contents in all samples analysed. Moreover, the XRD analysis identified sphalerite (ZnS), wurtzite ((Zn,Fe) S, quartz ($SiO_2$), calcite ($CaCO_3$), willemite ($Zn_2SiO_4$), cristobalite ($SiO_2$), zincite ($(Zn,Mn^{2+})O$, bytownite (Ca, Na)$[Al,Si)_4O_8$), kalicinite ($KHCO_3$), diopside ($CaMgSi_2O_6$), arcanite ($K_2SO_4$), chromite ($FeCr_2O_4$), microcline ($KAlSi_3O_8$), albite intermediate ($NaAlSi_3O_8$), and gypsum ($CaSO_4.2H_2O$) present in other samples.

The appearances of quartz and amorphous material in samples A, H, and ARC1, and their STACCs are associated with reactive silica, carbon black, rubber, organic additives (antioxidants and aromatic oil) contained in the spent tyre samples (Mavukwana, Celesti, 2022). In addition, the formation of either wurtzite, sphalerite, zincite, or willemite in these samples are ascribed to the interaction of inorganic additives (zinc metal or ZnO, $SiO_2$, sulphur; iron metal, Mn, Mg, and Si from steel wire) originally contained in TC at elevated activation temperatures under inert atmosphere (Maapola, 2019; Rodriguez et al., 2017). Furthermore, Agblevor et al. (2024) stated that wurtzite and sphalerite are formed via the in situ desulphurisation reaction between ZnO and metal sulphides in chars during pyrolysis.

A corrosion product identified such as chromite contained in the ARC1 sample could be due to the reaction between the stirrer equipment and AR at elevated temperature during the activation tests. Therefore, the high percentage ash yields present in the TC and its TC-derived activated chars are attributed to a significant mineral content in the TC samples detected by XRD (Table 4). These XRD results are consistent with the XRD data previously reported by Lopez et al. (2013).

## X-ray diffraction crystallite size analysis

The x-ray diffraction (XRD) analysis was followed to identify

*Table 4*

**Average XRD results of AC and A, and H and ARC1 (wt. %)**

| Mineral (wt. %) | AC | A | H | ARC1 |
|---|---|---|---|---|
| Quartz | 5.0 | 7.8 | 8.1 | 0.7 |
| Wurtzite 2H | 0.0 | 3.7 | 1.3 | 0.0 |
| Kalicinite | 0.0 | 0.0 | 0.0 | 0.0 |
| Diopside | 0.0 | 0.0 | 0.0 | 0.0 |
| Arcanite | 0.0 | 0.0 | 0.0 | 1.6 |
| Chromite | 0.0 | 0.0 | 0.0 | 14.8 |
| Microcline | 0.0 | 0.0 | 0.0 | 1.8 |
| Albite intermediate | 0.0 | 0.0 | 0.0 | 1.6 |
| Gypsum | 0.0 | 0.0 | 0.0 | 0.0 |
| Sphalerite | 0.0 | 9.8 | 0.6 | 0.0 |
| **MM** | **5** | **21.3** | **10.0** | **20.5** |
| **Amorphous material** | **95.0** | **78.7** | **90.0** | **79.4** |
| **Total** | **100.0** | **100.0** | **100.0** | **99.9** |

MM= total mineral matter

*Table 5*

**Qualitative XRD results of STACCs**

| Sample ID | Minerals |
|---|---|
| TC1 | Sphalerite, quartz, calcite, bytownite |
| TC2 | Wurtzite, quartz |
| TCA2 | Sphalerite, wurtzite, quartz, calcite, willemite, cristobalite, zincite |

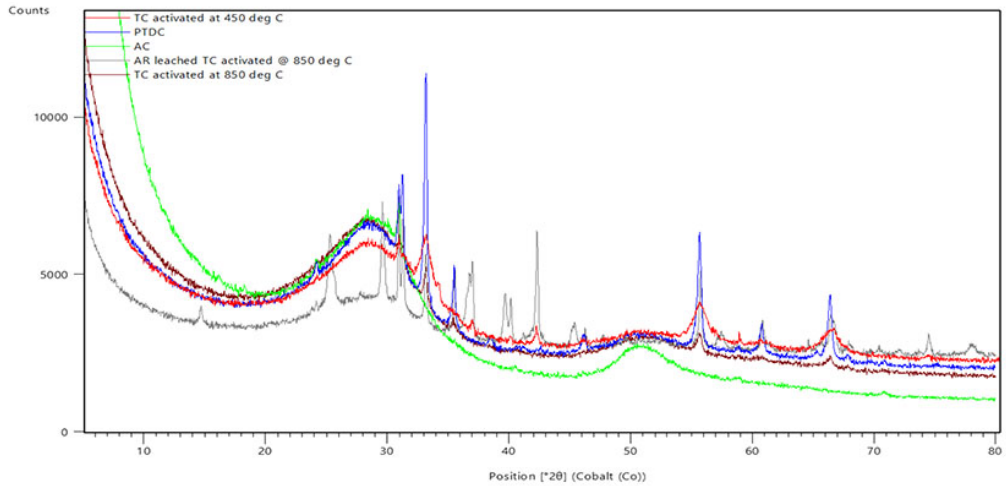


**Figure 3—XRD diffractograms for AC and spent tyre derived ACCs**

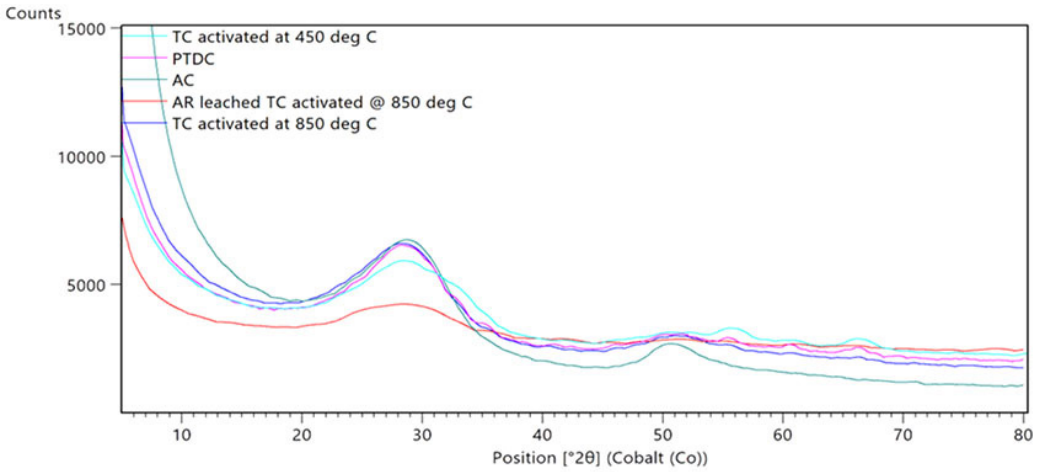


**Figure 4—Diffractograms of AC and South African spent tyre-derived ACCs**

both crystalline and amorphous carbons present in the AC and STACCs (PTDC and TC) produced using both physical and chemical activation methods. XRD results (Table 6) indicated that the STACCs prepared at 850°C depict a diffraction peak (002) around 2θ = 29° and peak (100) around 2θ = 52°, which are similar to those of AC (Figure 4). These XRD results are consistent with those reported in literature (Jin et al., 2016). While the TC-derived activated char, which was prepared at 450°C illustrates a diffraction peak (002) with no diffraction peak (100) due to the evolvement of carbon structures during the leaching of TC with AR. Also, the crystal structure of carbon in the analysed solid sample has an insignificant number of atoms arranged to generate a strong diffraction signal from that particular crystal plane; basically, the "100" plane is not apparent (Kittel, 2005). So, this plane is difficult to be detected in the diffraction data. From the diffractograms in Figure 4 it is apparent that both AC and STACCs produced at 850°C display a broad graphitic stacking signal at 2θ = 29° and a broad weak signal at 52°.

The diffraction peaks at 2θ = 29° and 2θ = 52° are linked to the (002) and (100) planes of the graphitic carbon, which are typically amorphous structures in nature (Ali et al., 2022; Ahmed et al., 2023; Bakti et al., 2023). The crystallite size value of either AC or STACCs was calculated by the Scherrer equation to be around 1 (Table 6) (Mphahlele et al., 2023). Based on the XRD results obtained for AC and STACCs containing both crystalline and amorphous carbons, it is proposed that these samples could be utilised in adsorption processes for removal of organic matter impurities from wastewater.

## Scanning electron microscopy morphology analysis

The scanning electron microscopy (SEM) micrographs of AC and TC, TCA and A, and their STACCs are displayed in Figure 5. The images of non-activated samples remained intact with surface smoothness of TC and TCA particles. Moreover, the SEM micrographs indicate that no formation of sufficient hollow spherical particles resembling "cenospheres" are present in the non-activated samples when matched with those of the STACCs. Furthermore, the pore structure development was not visually observed in all non-activated samples with respect to surface smoothness. While the SEM image of the

*Table 6*
**Average crystallite size of carbon in AC and STACCs**

| Sample | Bragg angle ($\theta$) (°) | $\beta$ (°) | Crystal size(D) (nm) |
|---|---|---|---|
| TC1 | 29.4 | 9.8 | 1.0 |
| A | 28.8 | 8.7 | 1.2 |
| AC | 29.3 | 8.7 | 1.2 |
| TCA2 | 28.3 | 8.6 | 1.2 |
| TC2 | 28.8 | 9.2 | 1.1 |

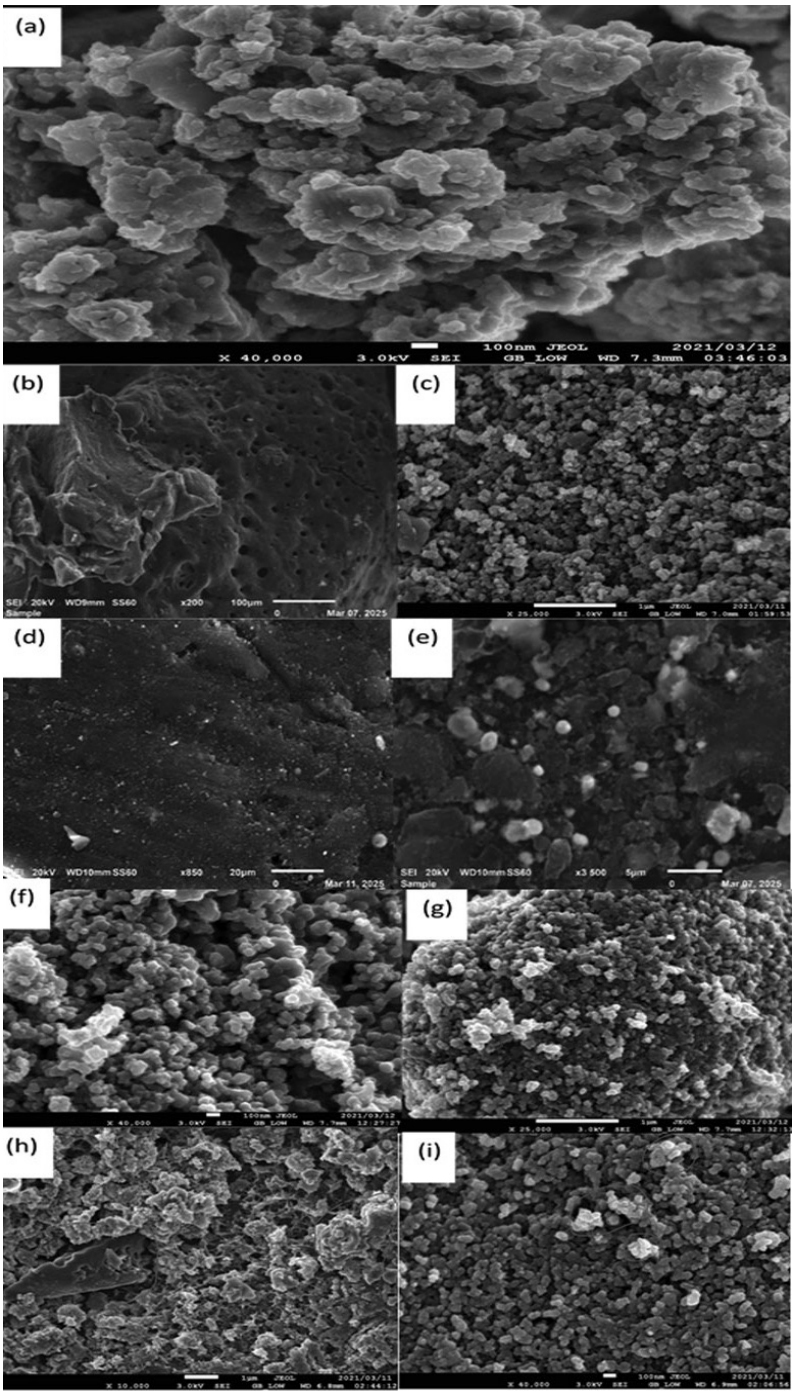


**Figure 5—The SEM images of (a) AC at 25 000× magnification, (b) TCA at 200× magnification, (c) TCA2 at 25 000× magnification, (d) TC at 850× magnification, (e) TC2 at 200× magnification, (f) ARC1 at 40000× magnification, (g) ARC2 at 25000× magnification, (h) A at 10 000× magnification, and (i) PTC2 at 40000× magnification**

TC sample demineralised with AR shows some surface roughness of TCA with cracks and holes. The appearances of the surface roughness, cracks, as well as the holes for TCA could be attributed to the release of volatiles (gases) emanating from either the partial decomposition of mineral matter or organic matter in Sample TC during demineralisation. The surface roughness of TCA may be associated with the exhibition of a higher SA of 300 $m^2/g$ during the TCA activation. Strydom et al. (2011) confirmed the distortion of the coal chemical structure, increased surface roughness, disordered crystalline carbon, and high aromatic compounds contents in the coal treated with inorganic acids. Also, the appearances of cracks and holes on the demineralised coals are ascribed to the volatilisation of $H_2$, $CH_4$, $CO_2$, $C_2H_4$, $C_2H_6$, $C_3H_4$, $C_3H_6$, and $C_4S$ from coals during either demineralisation or pyrolysis (Strydom et al., 2011).

Interestingly, all STACCs are made up of spherical particles as well as agglomerated spherical particles compared with those of the AC sample (Figure 5). In addition, the SEM micrograph, Figure 5(h) of A produced at 450°C, revealed that a piece remnant of TC, which is not present in ARC2 (prepared at 850°C), was still contained in these STACCs. Visual observation of the SEM image of AC (Figure 5 (a) indicated that all particles, which contained pores in this sample

were ruptured to form irregular shaped particles, which increased in size. These spherical particles containing trapped gases from the decomposition of minerals and organic matter started to rupture at elevated activation temperatures of 650°C and 850°C. Additionally, pores associated with high surface area and increased particle sizes were developed to form roughness in the activated chars after rupturing of the particles. The morphology analysis results of STACCs are consistent with those reported by Nagalakshmi et al. (2015). The amorphous cenospheres or spherical particles can be formed when emitted gases from the decomposition of minerals (either calcium/magnesium sulphate, kaolinite, calcite, dolomite or pyrite) present in the coal char particle inflated the partially melted inorganic mineral matter or the molten solution during combustion (Ranjbar, Kuenzel, 2017). The decomposition temperature of these coal minerals to release gases for inflation of spherical particles occurs at below 1000°C. On cooling, the molten solution produced at < 1000°C to 25°C, small hollow spherical particles (cenospheres) with diameters of 10 µm –1000 µm are formed. Cenospheres mainly comprise of alumino-silicate glasses with K, Na, Fe, Mg, Ca, Ti, and S. Therefore, two spherical particles coalesced with each other to form enlarged spherical particles (large agglomerates) (Ahmed et al., 2023; Ranjbar, Kuenzel, 2017).

Also, according to Tsemane et al. (2019), the < 1.3 g/cm$^3$ coal float fraction-derived char particles containing a high vitrinite content, which is associated with inherent kaolinite softened, swelled, melted, and formed big cakes or agglomerates at 550°C at pressures ranging between 0.87 bar and 30 bar during pyrolysis of caking coal.

The morphology results provide an insight into the physical properties of suitable STACCs for utilisation in the wastewater treatment plant following the adsorption process.

## Raman analysis

Figure 6 shows (a) the Raman spectra of AC, ARC1, (b) curve fitting of AC, and (c) curve fitting of ARC2. Figure 6a shows Raman spectra of sample AC being the highest due to a higher amorphous carbon content when compared to ARC1. Both spectrums are made of two relatively broad D-bands and G-bands, with spectra peaking near 1250 cm$^{-1}$ and the other band peaking up near 1500 cm$^{-1}$, respectively. The peak position of the D-band is approximately 1350 cm$^{-1}$, which mainly represents the defect structures in amorphous carbonaceous material and aromatics with 6 or more fused rings, while that of the G-band are approximately 1600 cm$^{-1}$. This represents the amorphous carbon with smaller aromatic ring structure. Similar Raman spectroscopy results for other waste tyre samples are reported by Kumar and Sharma (2018). The presence of defective carbon structure obtained at higher temperatures correlating with an increased aromatic structure formation, where the crystallisation of sp$^2$ amorphous carbon creates graphic networks as the temperature is raised was shown (Zhang et al., 2018). The wide D and G-band can also be corroborated with the presence of more surface functional groups such as thiophilic carbon, which influences the performance of carbon (Hood et al., 2018). Similar results were achieved by Zhang et al. (2011) using the gasification of steam with coal. These findings are consistent with the XRD results (amorphous phases) (Tables 4 and 5 and Figures 3 and 4) as reported in this study. Figure 6b and Figure 6c show the typical measured Raman spectrum and the four fitted peaks of AC and ARC2 located in the spectral range of 900 cm$^{-1}$ and 1800 cm$^{-1}$ deconvoluted using the curve fitting method. The use of the minor bands allows for the reduction of the

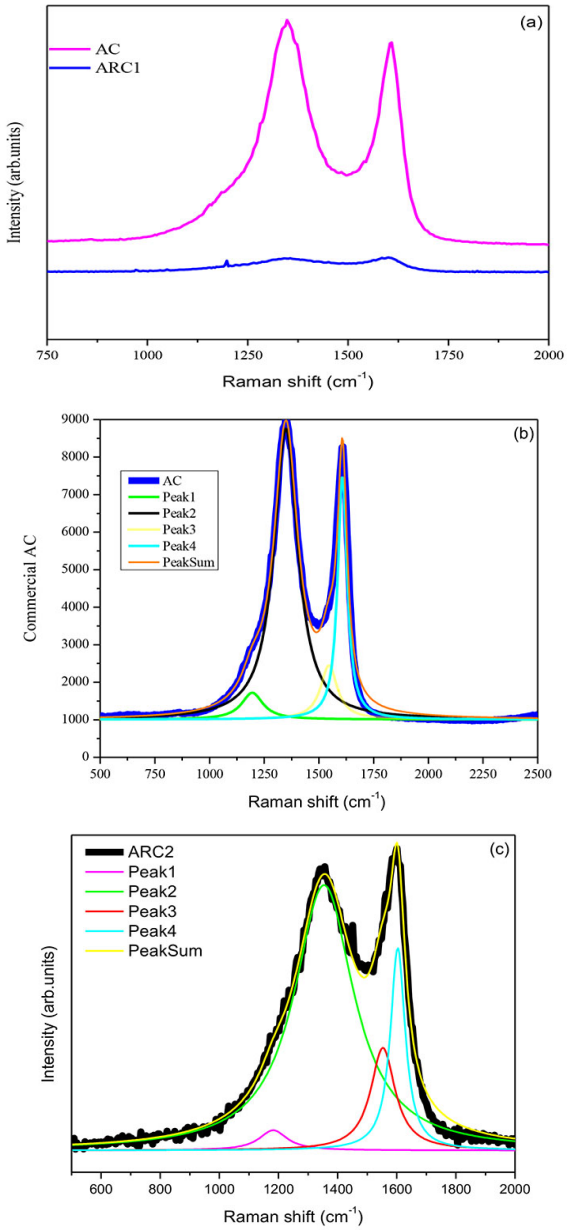


**Figure 6—Normalised Raman spectra for (a) curve fitting of AC and ARC1, (b) curve fitting of ARC2, (c) curve fitting of ARC2**

widths of the main bands. The wide D-bandwidths after spectral devolution indicate the presence of aromatic rings of a wide range of sizes but still far from forming graphite crystals (Li, Hayashi, Li, 2006). The growth in aromatic rings in the samples could be as a result of thermal activation of char over the temperature range. Also, the XRD crystallite size analysis results reveal that the crystallite size of the graphitic/crystalline carbon contained in AC and STACCs is around 1 nm (Table 6 and Figure 4). All other activated samples investigated in this study showed a similar success of peak fitting.

## Brunauer-Emmett-Teller surface area and pore volume characteristics

$N_2$ Brunauer-Emmett-Teller surface area (BET) surface area (SA) and pore volume (PV) results for samples labelled AC, TC, A, and their corresponding STACCs are presented in Figure 7 and Table 7. As expected, the commercial control AC sample contains relatively higher SA in relation to all samples and their STACCs produced

in this study. On the other hand, the TCA2 and TC2 samples had the highest PV when compared to all the STACCs, including AC. In addition, the TCA2 and TC2 samples comprised the highest SA, aligned with those of all samples analysed, excluding AC. The high SA results achieved by the STACCs (TCA2, TC2, and ARC1) could be attributed to a significant devolatilisation of volatile compounds from the reactive acidic sites of TCA, TC, and ARC during activation. According to Koreňová et al. (2008), the increase in the SA of tyre char is ascribed to an increase of voids, which takes place when volatiles are released from amorphous material. These SA and PV results obtained for the STACCs (excluding TCA2 and TC2) are similar to data for tyre-derived ACCs reported by Miguel, Fowler and Sollars (1998), Koreňová et al. (2008), and Li et al. (2005).

On the other hand, chars (PTC1, PTC2, ARC1, and ARC2) all showed a decrease in SA values with an increase in temperature from 450°C to 850°C, which indicates collapsing of mesopores during pyrolysis. Additionally, Howaniec (2016) found in their studies that the volume of macropores augmented at elevated temperatures and the SA of micropores decreased with rising temperature. Furthermore, the collapse of pores in materials, which result in low SA of chars can take place due to volatiles decomposition, mineral matter and organic matter transformation, atoms with increased mobility, thermal stress/expansion and contraction, pore size and volume dependence, and hotspot formation during activation of samples at elevated temperatures. Based on the characterisation results obtained in this study, the activated carbons with high contents of BET SA, PV and carbon could be utilised in adsorption processes to recover either high values metallic inorganic elements or impurities from leach liquors and wastewaters.

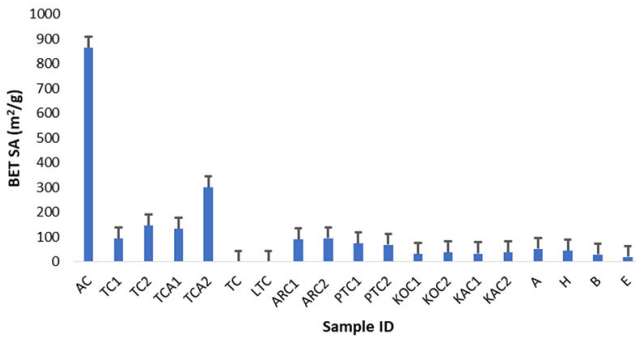


**Figure 7—Average SA values of AC and H, TC, TCA, and their STACCs**

*Table 7*

**Average PV of (a) AC, TC, TCA, A and H and their corresponding STACCs**

| Samples ID | Maximum PV at p/p° ($cm^3/g$) |
|---|---|
| AC | 0.4 |
| TC1 | 0.7 |
| TC2 | 0.8 |
| TCA2 | 0.5 |
| TC | <0.1 |
| TCA | <0.1 |
| ARC1 | 0.2 |
| ARC2 | <0.1 |
| PTC1 | <0.1 |
| PTC2 | <0.1 |
| A | <0.1 |
| H | <0.1 |

## Total organic carbon analysis

From Table 8 it is clear that the total organic carbon (TOC) content in the starch wastewater (SWW) sample significantly reduced from 25,365 ppm to 4,564 ppm in its effluent after the adsorption experiments of removing organic pollutants from SWW using a packed bed of commercial activated carbon (AC). Effluents generated from the different packed beds in the adsorption column with STACCs comprised higher TOC contents compared to that of the effluent produced from the packed-bed with AC. This implies that the AC adsorbent captured a significant quantity of these SWW organic contaminants (adsorbates) on its surface compared to other adsorbents evaluated in this study. The observed drop in TOC content indicates the successful transfer of organic compounds (adsorbates) from the liquid SWW phase to the surface of the solid AC adsorbent. This AC material with high SA, tailored PV structure, and functionalised surface may trap contaminants efficiently when SWW passes through a packed-bed of this adsorbent. The superior performance of AC is attributed to its high SA, PV structure, and functionalised surface, which enhance its capacity to trap contaminants (Muttil et al., 2023; Kuśmierek et al., 2021; Frikha et al., 2022; Satyam, Patra, 2024; Jiang et al., 2024).

The adsorption performance of the prepared STACCs in treating starch wastewater is summarized in Table 8. Based on the mass-balance calculations already described, TCA2 demonstrated a significant adsorption capacity of approximately 120 mg/g (assuming $C0$ = 2000 mg/L), achieving a 60% removal efficiency.

While the commercial AC reached a higher removal efficiency (92%), the performance of TCA2 is particularly noteworthy given its origin as a waste-derived material. The depth of this adsorption is attributed to the high pore volume (0.8 $cm^3/g$), which facilitates the sequestration of complex starch molecules as supported by the SEM analysis discussed in the aforementioned.

## Adsorption studies of the capacity of prepared chars

Figure 8 presents the TOC removal efficiency in SWW using AC and STACCs (PTC2, ARC2, TC2, and TCA2) with high BET SA, PV values, and low mineral matter content as adsorbents. The highest TOC removal efficiency was achieved by AC due to its highest SA area (865 $m^2/g$), higher PV (0.4 $cm^3/g$), and lowest mineral matter content (5%) (Tables 4 and 8). On the other hand, TCA2

*Table 8*

**TOC contents for SWW and their effluents after using packed-beds with AC and STACCs (ppm)**

| Samples | Test 1 | Test 2 | Test 3 | Average TOC content |
|---|---|---|---|---|
| SWW | 26447 | 25161 | 26447 | 25365 |
| AC-SWW | 4818 | 5325 | 4057 | 4564 |
| TCA2-SWW | 7607 | 8621 | 8114 | 8114 |
| TC2-SWW | 11664 | 11664 | 10143 | 11157 |
| ARC2-SWW | 14453 | 15468 | 15721 | 15214 |
| PTC2-SWW | 19018 | 20793 | 20032 | 20032 |

Note: SWW is starch wastewater, AC-SWW is the effluent produced from a packed-bed with the AC during the adsorption test, TCA2-SWW is the effluent produced from a packed-bed with TCA2 during the adsorption test, TC2-SWW is the effluent produced from a packed-bed with TC2 during the adsorption test, ARC2-SWW is the effluent produced from a packed-bed with ARC2 during the adsorption test, and PTC2-SWW is the effluent produced from a packed-bed with PTC2 during the adsorption test.

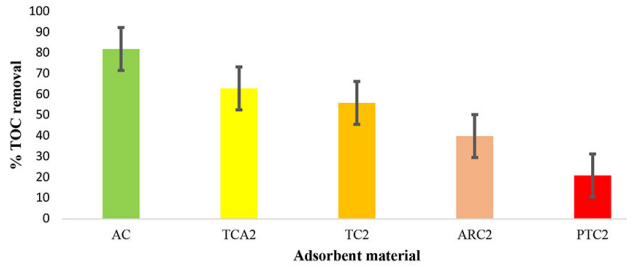


**Figure 8—Average TOC removal efficiency percentage using AC and STACCs**

with a higher SA (300 $m^2/g$) and a higher PV (0.5 ($cm^3/g$) as well as a lower percentage ash yield accomplished a higher percentage removal efficiency of TOC aligned with those of other STACCs. Furthermore, TCA and TC2 exhibited a higher proportion of PV characteristic, which were developed during activation, than that of AC. There is a difference of 20% removal efficiency of TOC from SWW between TCA2 and AC. This may imply that the developed higher PVs in the STACCs play a more important role rather than the SA during adsorption of TOC in SWW. Therefore, TCA2 with SA (300 $m^2/g$) and PV of 0.8 $cm^3/g$ has good adsorption capacity for TOC, favourably comparable with that of AC. These higher SA values of TCA2 that achieved good adsorption efficiencies of organic pollutants are consistent with those reported by Kuśmierek, et al. (2021), Ali et al. (2022) and Mohammed et al. (2023), and Jiang et al. (2024). Additionally, Helleur et al. (2001) stated that the BET SA of pores do not always support the advancement of adsorption capacity of activated carbons, which indicates that the porosity characteristics, rather than the SA, acted a key role in the adsorption capacity of STACCs.

PTC2 had the smallest SA (70 $m^2/g$) and the lowest PV (0.03 $cm^3/g$), which explains the reason why the removal efficiency of TOC was the lowest (Figure 8). However, the ARC2 has proven to be the most effective when it removes almost double (40% for ARC2 vs. 21% for PTC2) the amount of TOC matched with PTC2. TCA2 and TC2 produced from TC material outperformed those of PTDC material in terms of both SA and PV and an excellent adsorption of TOC in SWW. The adsorption results for TOC from SWW using STACCs are in good agreement with those reported by Helleur et al. (2001).

## Conclusions

This study successfully demonstrated the technical and environmental viability of transforming waste tyre rubber into high-performance activated carbon chars (STACCs). Characterisation through SEM, XRD, and Raman spectroscopy confirmed that physical activation (temperature) at 850°C, preceded by an aqua regia demineralisation step, yields an amorphous carbon matrix with superior textural properties. Specifically, the prepared TCA2 adsorbent achieved a surface area of 300 $m^2/g$ and a pore volume of 0.8 $cm^3/g$—effectively doubling the pore volume of commercial activated carbon (0.4 $cm^3/g$).

These structural attributes directly influenced the treatment of high-strength starch wastewater, where TCA2 achieved a 60% Total Organic Carbon (TOC) removal efficiency. As elucidated in Figure 5, the synergistic adsorption pathways—driven primarily by pore-filling and electrostatic interactions—allow these waste-derived chars to target complex organic molecules that typically challenge standard filtration media.

The primary novelty of this investigation lies in the successful conversion of an environmental liability (waste tyres) into a high-pore-volume adsorbent that rivals commercial standards in treating actual industrial starch effluents. By decoupling the effects of demineralisation and physical activation, this work provides a scalable blueprint for localised circular economy implementation. Ultimately, this research offers a sustainable dual pathway for South African industries, that is, mitigating the ecological burden of tyre stockpiles while significantly reducing the costs associated with industrial wastewater remediation.

## Glossary

| Abbreviations | Definition |
|---|---|
| PTDC | Pyrolytic spent tyre-derived char |
| STACCs | Spent tyre-derived activated carbon chars |
| TOC | Total organic carbon |
| TC | Spent tyre crumb rubber |
| TC2 | TC heated to 850°C (char) |
| TC1 | TC heated to 650°C (char) |
| TCA | TC leached with aqua regia |
| TCA2 | TCA heated to 850°C (char) |
| AC | Commercial activated carbon |
| SWW | Starch wastewater |
| SS | Suspended organic solids |
| SA | Surface area |
| PV | Pore volume |
| ACC | Activated carbon chars |
| PSD | Particle size distribution |
| Macro-TGA | In-house developed macro thermogravimetric analysis system |
| BET | Brunauer-Emmett-Teller |
| XRD | X-ray diffraction |
| XRF | X-ray fluorescence |
| SEM | Scanning electron microscopy |
| AR | Aqua regia |
| MINTEK | Mineral Technology |
| FWHM | Full width at half-maximum |
| CSIR | Council for Scientific and Industrial Research |
| VM | Volatile matter |
| SCC | Spent carbon char/s |
| TS | Total sulphur |
| SARChI | South African Research Chairs Initiative |
| MM | Total mineral matter |
| NRF | National Research Foundation |
| PAH | Polycyclic aromatic hydrocarbons |
| Daf | Dry ash-free basis |
| Adb | Air-dried basis |
| IM | Inherent moisture |
| AY | Ash yield |
| FC | Fixed carbon |
| PTC2 | PTDC heated to 850°C (char) |
| PTC1 | PTDC heated to 650°C (char) |
| H | PTDC leached with aqua-regia |
| ARC1 | ARC heated to 650°C (char) |
| ARC2 | ARC heated to 850°C (char) |
| A | PTDC |

## Acknowledgements

This paper was financially supported by the Vaal University of Technology, Department of Chemical Engineering, Vanderbijlpark, South Africa, and the National Research Foundation (NRF), South Africa. The information presented in this paper is based on the research financially supported by the South African Research Chairs Initiative (SARChI) of the Department of Science and Technology and NRF of South Africa (Coal Research Chair Grant No. 86880). Any opinion, finding, conclusion or recommendation expressed in this material is that of the author(s) and the NRF does not accept any liability in this regard. Also, the authors would like to express their appreciation to NRF free-standing bursary MND200715544211/UID: (136078) for the financial contributions. The authors would like to acknowledge Energy Partners, Alrode, South Africa and UDEC trading (Pty) LTD, Kempton Park, Johannesburg, South Africa for provision of PTDC and commercial activated carbon. Also, Roy Mamburu (MINTEK) for making the TGA available. Willem Swanepoel of Bureau Veritas, Dr Gregory Okolo of the North-West University, Nomsa Mavundla of Ingrain SA Germiston mill and Dr Liberty Kapesi for rendering excellent laboratory services.

## References

Abbas-Abadi, M.S., Kusenberg, M., Shirazi, H.M., Goshayeshi, B., Van Geem, K.M. 2022. Towards full recyclability of end-of-life tyres: Challenges and opportunities. *Journal of Cleaner Production* vol. 374, pp.134036, https://doi.org/10.1016/j.jclepro.2022.134036

Agblevor, F.A., Hietsoi, O., Jahromi, H., Abdellaoui, H. 2024. Production of low-sulphur fuels from catalytic pyrolysis of waste tyres using formulated red-mud catalyst. *Heliyon*, vol. 10, e33121. https://doi.org/10.1016/j.heliyon.2024.e33121

Ahmed, B., Arjmandi-Tash, O., Litster, J.D., Smith, R.M. 2023. Mechanistic modelling of spherical agglomeration processes. *Powder Technology*, vol. 417, pp.118254. https://doi.org/10.1016/j.powtec.2023.118254

Ali, I., Asim, M., Khan, T. 2012. Low cost adsorbents for the removal of organic pollutants from wastewater. *Journal of Environmental Management*, vol. 113, pp. 170–183, 105205. https://doi.10.1016/j.jenvman.2012.08.028

Ali, U.F.M., Hussin, F., Gopinath, S.C.B., Aroua, M. K., Khamidun, M.H., Jusoh, N., Ibrahim, N., Ahmad, S.F.K. 2022. Advancement in recycling waste tyre activated carbon to potential adsorbents. *Environmental Engineering Research,* vol. 27, no. 6. pp. 210452. https://doi.org/10.4491/eer.2021.452

Aoyi, O., Onyango, M.S., Apollo, S., Akach, J., Nyembe, N., Oteno, B., Brooms, T. 2017. Anaerobic and photocatalytic treatment of textile and distillery wastewater in integrated fluidized bed reaction. Water Research Commission, Centre for Renewable Energy and Water, Vaal University, WRC Report No. 2388/1/18, ISBN 978-1-4312-0998-9.

Ayaz, M., Shah, S.S., Younas, M., Safder, U., Khan, I., Aziz, M.A., Oyama, M., Rice, J.H., Tahir, M.N., Ashraf, M. 2025. Green synthesis of activated carbon from biomass waste of date palm seeds: A sustainable solution for energy storage and environmental impact. *Journal of Energy Storage*, vol. 110, pp. 115291. https://doi. 10.1016/j.est.2025.115291

Bai, J., Zhang, X., Wang, C., Li, X., Xu, Z., Jing, C., Zhang, T., Jiang, Y. 2024. The adsorption-photocatalytic synergism of LDHs-based nano-composites on the removal of pollutants in aqueous environment: A critical review. *Journal of Cleaner Production*. vol. 436, pp.140705. https://doi. 10.1016/j.jclepro.2024.140705

Bakti, A.I., Mosey, H.I.R., Jumriadi, J. 2023. Characterisation and analysis of activated carbon from coconut shells applied to supercapacitors. *Sainstek Jurnal Sains dan Teknologi*, vol. 15, pp. 128. https://doi.10.31958/js.v15i2.10605

Baloyi, B.M.V., Chetty, D., Mchabe, D. 2025. Assessing the impact of prereduction parameters on Mn ore from the Kalahari Manganese Field. *Journal of the Southern African Institute of Mining and Metallurgy*, vol. 125, no. 3, pp. 121–128. https://doi.org/10.17159/2411-9717/770/2025

Carmona-Cabella, M., Garcia, I.L., Saez-Bastante, J., Pinzi, S., Koutinas, A.A., Dorado, M.P. 2020. Food waste from restaurant sector-characterization for biorefinery approach. *Bioresource Technology*, vol. 301, pp. 122779. https://doi.org/10.1016/j.biortech.2020.122779

Chen, J.P., Wu, S. 2004. Acid/base-treated activated carbons: Characterization of functional groups and metal adsorptive properties. *Langmuir*, vol. 20, pp. 2233–2242. https://doi.10.1021/la0348463

Cunliffe, A.M., Williams, P.T. 1998. Properties of chars and activated carbons derived from the pyrolysis of used tyres. *Environmental Technology*, vol. 19, pp. 1177–1190. https://doi.org/10.1080/09593331908616778

Daniel, L.S., Rahman, A., Hamushembe, M.N., Kapolo, P., Uahengo, V., Jonnalagadda, S.B. 2023. The production of activated carbon from Acacia erioloba seedpods via phosphoric acid activation method for the removal of methylene blue from water. *Bioresource Technology Reports*, vol. 23, pp. 101568. https://doi.org/10.1016/j.biteb.2023.101568

Danish, M., Hashim, R., Mohamad Ibrahim, M.N., Sulaiman, O. 2013. Effect of acidic activating agents on surface area and surface functional groups of activated carbons produced from Acacia Mangium wood. *Journal of Analytical and Applied Pyrolysis*, vol. 104, pp. 418–425. https://doi.org/10.1016/j.jaap.2013.06.003

Frikha, K., Limousy, L., Pons Claret, J., Vaulot, C., Perez, K.F., Garcia, B.C., Bennici, S. 2022. Potential valorisation of waste tyres as activated carbon-based adsorbent for organic contaminants removal. *Materials*, vol. 15, pp. 1099. https:// doi.org/10.3390/ma15031099

Gorito, A.M., Ribeiro, A.R., Gomes, C.R., Almeida, M.R., Silva, A.M.T. 2018. Constructed wetland microcosms for the removal of organic micropollutants from freshwater aquaculture effluents. *Science of the Total Environ*, vol. 644, pp.1171–1180. https://doi. 10.1016/j.scitotenv.2018.06.371

Han, W., Han, D., Chen, H. 2023. Pyrolysis of waste tyres: A review. *Polymers*, vol. 15, pp.1604. https://doi.org/10.3390/polym15071604

He, L., Ma, Y., Liu, Q., Mu, Y. 2016. Surface modification of crumb rubber and its influence on the mechanical properties of rubber-cement concrete. *Construction and Building Materials.* vol.120, pp. 403–407. https://doi. 10.1016/j.conbuildmat.2016.05.025

Helleur, R., Popovic, N., Ikura, M., Stanciulescu, M., Liu, D. 2001. Characterization and potential applications of pyrolytic char from ablative pyrolysis of used tyres. *Journal of Analytical and Applied Pyrolysis*. vol. 58, pp. 813–824. https://doi.org/10.1016/S0165-2370(00)00207-2

Hood, Z.D., Yang, X., Li, Y., Naskar, A.K., Chi, M., Paranthaman, M.P. 2018. Conversion of waste tyre Rubber into high-value-added carbon supports for Electrocatalysis. *Journal of Electrochemical Society*. vol. 165, pp. 881–888. https://doi. 10.1149/2.1081813jes

Howaniec, N. 2016. Temperature development of porous structure of bituminous coal chars at high pressure. *Journal of Sustainable Mining*. vol. 15, pp. 120–124. https://doi.org/10.1016/j.jsm.2016.12.002

Igwegbe, C. A., Umembamalu, C. J., Osuagwu, E. U., Oba, S. N., Emembolu, L. N. 2021. Studies on adsorption characteristics of corn cobs activated carbon for the removal of oil and grease from oil refinery desalter effluent in a downflow fixed bed adsorption equipment. *European Journal of Sustainable Development Research*, vol. 5, no. 1. em0145. https://doi.org/10.29333/ejosdr/9285

Jiang, S., Lyu, Y., Zhang, J., Zhang, X., Yuan, M., Zhang, Z., Jin, G., He, B., Xiong, W., Yi, H. 2024. Continuous adsorption removal of organic pollutants from wastewater in a UiO-66 fixed bed column. *Journal of Environmental Chemical Engineering,* vol. 12, no. 2, pp. 111951. https://doi.org/10.1016/j.jece.2024.111951

Jin, Y., Tian, K., Wei, L., Zhang, X., Guo, X. 2016. Hierarchical porous microspheres of activated carbon with a high surface area from spores for electrochemical double-layer capacitors. *Journal of Materials Chemistry*, vol. 4, pp. 15968–15979. https://doi.org/10.1039/C6TA05872H

Kapesi, L. 2018. Promoting carbon nanotube interlinking using ion implantation and high pressures in a diamond Anvil cell. *Master's Dissertation*, University of Johannesburg, Johannesburg, South Africa. pp. 19–35.

Kittel, C. 2005. Introduction to solid state physics, 8th ed., ISBN 0-471-41526-X, WIE ISBN 0-471-68057-5, Printed in the United States of America, University of California, Berkeley, John Wiley & Sons, Inc. pp 3-22.

Koreňová, Z., Haydary, J., Annus J., Markoš, J., Jelemenský, L. 2008. Pore structure of pyrolysed scrap tyres. *Chemical Papers* vol. 62, pp. 86–91. https://doi.org/10.2478/s11696-007-0083-7

Kumar, R., Sharma, A. 2018. Morphologically tailored activated carbon derived from waste tyres as high-performance anode for Li-ion battery. *Journal of Applied Electrochemistry*. vol. 48, pp. 1–13. https://doi.10.1007/s10800-017-1129-3

Kuśmierek, K., Świątkowski, A., Kotkowski, T., Cherbanski, R., Molga, E. 2021. Adsorption on activated carbons from end-of-life tyre pyrolysis for environmental applications. Part II. Adsorption from aqueous phase. *Journal of Analytical and Applied Pyrolysis*, vol.158, pp. 105206, https://doi 10.1016/j.jaap.2021.105206

Li, S.-Q., Yao, Q., Wen, S.-E., Chi, Y., Yan, J.-H. 2005. Properties of pyrolytic chars and activated carbons derived from pilot-scale pyrolysis of used tyres. *Journal of the Air and Waste Management Association*, vol. 55, pp.1315–1326. https://doi.org/10.1080/10473289.2005.10464728

Li, X., Hayashi, J-I., Li, C-Z. 2006. FT-Raman spectroscopic study of the evolution of char structure during the pyrolysis of a Victorian brown coal. *Fuel*, vol. 85, pp. 1700–1707. https://doi.10.1016/j.fuel.2006.03.008

Liu, L., Zhang, J., Liu, X., Cai, G. 2020. Evaluation of engineering properties and environmental effect of recycled waste tyre-sand/soil in geotechnical engineering: A Compressive Review. *Renewable and Sustainable Energy Reviews*, vol. 126, pp. 109831. https://doi.org/10.1016/j.rser.2020.109831

Lopez, A.F., Centeno, T.A., Alguacil, F.J., Lobato, B., Urien, A. 2013. The Grauthermic-tyres process for the recycling of granulated scrap tyres. *Journal of Analytical and Applied Pyrolysis*, vol. 103, pp. 207–215. https://doi.10.1016/j.jaap.2012.12.007

Maapola, T.T.P. 2019. Evaluation of waste tyre-derived char and crumb as adsorbents for gold recovery from acidic solutions. *Master of Chemical Engineering*, Stellenbosch University. pp. 5–146.

Maroufi, S., Mayyas, M., Sahajwalla, V. 2017. Nano-carbons from waste tyre rubber: An insight into structure and morphology. *Waste Management*, vol. 69, pp. 110–116. https://doi: 10.1016/j.wasman.2017.08.020

Mavukwana, A., Celesti, S. 2022. Recent developments in waste tyre pyrolysis and gasification processes. *Chemical Engineering Communication*, vol. 209, pp. 485–511. https://doi. 10.1080/00986445.2020.1864624

Merchant, A. A., Petrich, M.A. 1993. Pyrolysis of scrap tyres and conversion of chars to activated carbon. *AIChE Journal*, vol. 39, pp. 1370–1376. https://doi.org/10.1002/aic.690390814

Miguel, G.S., Fowler, G.D., Sollars, C.J. 1998. Pyrolysis of tyre rubber: Porosity and adsorption characteristics of the pyrolytic chars. *Industrial and Engineering Chemistry Research*, vol. 37, no. 6, pp. 2430–2435. https://doi.org/10.1021/ie970728x

Mohammed, Z.J, Kadhim, F. Al-Sultani, K.F. 2023. Removal of Organic Pollutants from Wastewater by Column adsorption process using Corncob activated carbons as adsorbents. *Journal of University of Babylon for Engineering Sciences*, vol. 31, no. 8, pp. 130–144. https://doi.org/10.29196/pjc4s998

Mphahlele, K., Matjie, R.H., Bunt, J.R., Uwaoma, R. C. 2023. Properties and reactivity of two oxidized and unoxidized South African Highveld fine coal rejects and their density-separated fractions. *International Journal of Coal Preparation and Utilization*, vol. 43, no. 8, pp. 1451–1477. https://doi.org/10.1080/19392699.2023.2221634

Muttil, N., Jagadeesan, S., Chanda, A., Duke, M., Singh, S.K. 2023. Production, types and applications of activated carbon-derived from waste tyres: An Overview. *Applied Science*, vol. 13, no. 1, p. 257. https://doi.org/10.3390/app13010257

Muzenda, E. 2014. An evaluation of the effectiveness of the Gauteng Provincial Legislature's Infrastructure Development Portfolio Committee. *Unpublished Masters Dissertation.* Johannesburg: University of Johannesburg.

Nagalkshmi, T.V., Emmanuel, K.A., Babu, S., Challari, C., Divakar, P.P. 2015. Preparation of mesoporous activated carbon from Jackfruit PPL-1 waste and development of different surface functional groups. *International Letters of Chemistry, Physics and Astronomy*, vol. 54, pp. 189 –200. https://doi.10.56431/p-957378

Nkosi, N., Muzenda, E., Mamvura, T.A., Belaid, M., Patel, B. 2020. The development of a waste tyre pyrolysis production plant business model for the Gauteng region, South Africa. *Processes*, 8, 766. Processes, vol. 8, no. 7, pp. 766. https://doi.org/10.3390/pr8070766

Nkosi, N., Nhubu, T., Mthombeni, N.H. 2025. An inventory analysis of waste tyre generation and management in South Africa. *Waste Management,* vol. 194, pp. 353–365. https:// doi. 10.1016/j.wasman.2025.01.004

Norrish, K., Hutton, J.T. 1969. An accurate X-ray spectrographic method for the analysis of a wide range of geological samples. *Geochimica et Cosmochimica Acta*, vol. 33, no. , pp. 431–453. https://doi.org/10.1016/0016-7037(69)90126-4

Ozturk, I., Ersahin, M.E., Tezer, B.H. 2005. Pollution report of Cargill Orhangazi corn processing Factory. Istanbul Technical University, Istanbul, Turkey.

Patterson, A.L. 1939. The Scherrer Formula for X-Ray Particle Size Determination. *Physical Review*, vol. 56, pp. 978. https://doi.org/10.1103/PhysRev.56.978

Rambau, M.K., Musyoka, M.N., Manyala, N., Ren, J., Langmi, H.W. 2018. Mechanochemical approach in the synthesis of activated carbons from waste tyres and its hydrogen storage applications. *Materials Today Proceedings*, vol. 5, no. 4, 10505–10513. https://doi. 10.1016/j.matpr.2017.12.382

Ranjbar, N., Kuenzel, C. 2017. Cenospheres: A review. *Fuel*, vol. 207, pp. 1–12. https://doi.org/10.1016/j.fuel.2017.06.059

Rautenbach, R., Strydom, C.A., Bunt, J.R., Matjie, R.H., Campbell, Q.P., Van Alphen, C. 2019. Mineralogical, chemical, and petrographic properties of selected South African power stations' feed coals and their corresponding density separated fractions using float-sink and reflux classification methods. *International Journal of Coal Preparation and Utilization*, vol. 39, no. 8, pp. 421–446. https://doi.10.1080/19392699.2018.1533551

Rietveld, H.M. 1969. A Profile refinement method for nuclear and magnetic structures. *Journal of Applied Crystallography*, vol. 2, pp. 65–71. https://doi.org/10.1107/S0021889869006558

Rodriguez, O.O., Duque, W.O., Salazar, L.I. 2017. Environmental impact of end-of-life tyre: Life cycle assessment comparison of three scenarios from a case study in Valle Del Cauca, Colombia. *Energies*, vol. 10, no. 12, p. 2117. https://doi.org/10.3390/en10122117

Satyam, S., Patra, S. 2024. Innovations and challenges in adsorption-based wastewater remediation: A comprehensive review. *Heliyon*, vol. 10, no. 9, e29573. https://doi.org/10.1016/j.heliyon.2024.e29573

Scherrer, P. 1912. Determination of the internal structure and size of colloid particles by means of X-rays. In Kolloidchemie Ein Lehrbuch, ed. R. Zsigmondy. Berlin Heidelberg, Berlin, Heidelberg: Springer. pp. 387–409.

Seng-Eiad, S., Jitkarnka, S. 2016. Untreated and $HNO_3$-treated pyrolysis char as catalysts for pyrolysis of waste tyre: In-depth analysis of tyre-derived products and char characterization. *Journal of Analytical and Applied Pyrolysis*, vol. 122, pp. 151–159. https://doi.10.1016/j.jaap.2016.10.004

Speakman, S.A. 2012. Introduction to PANalytical X'Pert HighScore Plus v3. 0. Massachusetts: MIT Center for Materials Science and Engineering. pp. 1-19.

Stefanidis, S. D., Pachatouridou, E., Heracleous, E., Lappas, A.A., Vasalos, I.A. 2025. Chemical Recycling of End-of-Life Tyres Using Catalytic Pyrolysis: Effects of Catalysts and Process Conditions toward the Production of a Highly Aromatic Pyrolysis Oil. *Industrial & Engineering Chemistry*, vol. 64, no. 40, pp. 19342–19358. https:// doi.10.1021/acs.iecr.5c02163

Strydom, C.A., Bunt, J.R., Schobert, H.H., Raghoo, M. 2011. Changes to the organic functional groups of an inertinite-rich medium rank bituminous coal during acid treatment processes. *Fuel Process Technol.*, vol. 92, no. 4, pp. 764–770. https://doi:10.1016/j.fuproc.2010.09.008

Sugiati, Y., Nurmayani, S., Nailufhar, L., Tiyana, R., Nata, A.G. 2023. Chemical oxygen demand reduction and pre-treatment method of dairy industry sludge waste for lactic-acid fermentation purpose. *AIP Conference Proceedings*. 2646, No. 1.030012. https://doi. 10.1063/5.0113175

Tchobanoglous, G., Burton, F.L., Stensel, H.D. 2003. Wastewater engineering treatment and reuse. Fourth Ed. Metcalf and Eddy Inc., Mc-Graw-Hill, ISBN: 0-07- 041878-0, New York, USA.

Tsemane, M.M., Matjie, R.H., Bunt, J.R., Neomagus, H.W.J.P., Strydom, C.A., Waanders, F.B., Van Alphen, C., Uwaoma, R. 2019. Mineralogy and petrology of chars produced by South African caking coals and density-separated fractions during pyrolysis and their effects on caking propensity. *Energy & Fuels*, vol. 33, no. 8, pp. 7645–7658. https: //doi. 10.1021/acs.energyfuels.9b01275

Wang, T., Tan, S., Liang, C. 2009. Preparation and characterization of activated carbon from wood via microwave-induced ZnCl2 activation. *Carbon*, vol. 47, no. 7, pp. 1880–1883. https://doi. 10.1016/j.carbon.2009.03.035

Xiaowe, C., Sheng, H., Xiaoyang, G., Wenhui, D. 2017. Crumb waste tyre rubber surface modification by plasma polymerization of ethanol and its application on oil-well cement. *Applied Surface Science,* vol. 409, pp. 325–342. https://doi.org/10.1016/j.apsusc.2017.03.072

Yang, X., Kleinrahm, R., McLinden, M.O., Richter, M. 2020. Uncertainty analysis of adsorption measurements using commercial gravimetric sorption analyzers with simultaneous density measurement based on a magnetic suspension balance. *Adsorption*, vol. 26, no.4, pp. 645–659. https://doi.org/10.1007/s10450-020-00236-1

Yaru, S.S., Satope, P.O., Akinola, A.O. 2021. Characterization of char from waste tyre pyrolysis. *Saudi Journal of Engineering and Technology*, vol. 6, no. 7, pp. 169–177. https://doi. 10.36348/sjet.2021.v06i07.004

Yu, Y., Kil, H-S., Nakabayashi, K., Yoon, S-H., and Miyawaki, J. 2019. Toward development of activated carbons with enhanced effective adsorption amount by control of activation process, Conference: The 4th International Conference on Industrial Mechanical, Electrical, and Chemical Engineering, *AIP Conference Proceedings*, 2097(1): 020002. https://doi.10.1063/1.5098173

Zhang, P., Li, Y., Cao, Y., Han, L. 2019. Characteristics of tetracycline adsorption by cow manure biochar prepared at different pyrolysis temperatures. *Bioresour. Technol*, vol. 285, pp. 121348. https://doi.org/10.1016/j.biortech.2019.121348

Zhang, S., Min, Z., Tay, H-I., Asadulla H, M., Li, C-Z. 2011. Effects of volatile–char interactions on the evolution of char structure during the gasification of Victorian brown coal in Steam. *Fuel*, vol. 90, no. 4, pp. 1529–1535. https:// doi.10.1016/j.fuel.2010.11.010

Zhang, X., Li, H., Cao, Q., Jin, L., Wang, F. 2018. Upgrading pyrolytic residue from waste tyres to commercial carbon black. *Waste Management and Research*, vol. 36, no. 5, pp. 436–444. https:// doi. 10.1177/0734242X18764292

Zhang, M., QI, Y., Zhang, W., Wang, M., Li, J., Lu, Y., Zhang, S., He, J., Cao, H., Tao, X., Xu, H., Zhang, S. 2024. A review on waste tyres pyrolysis for energy and material recovery from the optimization perspective. *Renew. Sustain. Energy Rev.*, vol. 199, pp. 114531. https://doi.10.1016/j.rser.2024.114531

Zilli, M. 2013. A practical guide to the calculation of uncertainty of measurement. The Open Toxicology Journal, 2013, vol. 6, (Suppl 1, M3), pp. 20–26. ◆